PROCEEDINGS OF SCIENCE

The impact of the stellar wind on the non-thermal processes in gamma-ray binaries

Elina Kefala* **and Valentí Bosch-Ramon**

Departament de Física Quàntica i Astrofísica, Institut de Ciències del Cosmos (ICC), Universitat de Barcelona (IEEC-UB),
Martí i Franquès 1, 08028 Barcelona, Spain

E-mail: ekefala@icc.ub.edu, vbosch@fqa.ub.edu

This study investigates the dynamics and emission of rotation-powered gamma-ray binaries, which are characterized by the synergy between an energetic pulsar and a massive star. Utilizing a semi-analytical approach, we characterize the dynamics of the contact discontinuity and Coriolis shock resulting from the interaction between stellar winds and the pulsar wind. The model successfully reproduces the observed behavior of LS 5039 in X-rays and TeV gamma rays, clarifies the contribution of the two shock regions in the high-energy emission of gamma-ray binaries, and confirms the need for refined modeling to address the limitations of existing models in matching the $10-30$ MeV and $0.1-10$ GeV data.

High Energy Phenomena in Relativistic Outflows VIII (HEPROVIII)
23-26 October, 2023
Paris, France

*Speaker

PoS(HEPROVIII)069

1. Introduction

Gamma-ray binaries are typically the pairing of an energetic pulsar and a massive star. Their emission, peaking at MeVs and extending up to TeVs, is intricately tied to the orbital motion. This modulation is indicative of a connection between the binary dynamics and the production of high-energy gamma rays. Massive stars often have powerful winds composed of charged particles that are expelled from the stellar surface due to radiation pressure. In the wind-driven scenario of gamma-ray binaries, these stellar winds interact with the less powerful pulsar wind, which is fueled by the pulsar's spin-down, forming a double bow shock with a contact discontinuity. On large scales, orbital motion causes the pulsar wind to progressively "bend". The asymmetric wind–wind interaction produces a second shock at the Coriolis turnover location [1, 2]. The contact discontinuity and Coriolis shock are the primary locations for particle acceleration and non-thermal emission. In this study, we model the two shock regions semi-analytically and compute the non-thermal emission for LS 5039 to explain the observed spectral energy distributions and light curves.

2. Modeling the emitting region

For a static binary system, the shape of the contact discontinuity is determined by the balance condition of the ram pressures of the two winds [3, see their Eq. (26)]. The axisymmetric solution is modified to account for orbital effects by rotating the entire structure against orbital motion by an angle $\sim d\omega_{\rm orb}/u_{\rm w}$ with respect to the symmetry axis, where d is the orbital separation, $\omega_{\rm orb}$ is the angular velocity of the pulsar, and $u_{\rm w} = 2\times10^8$ cm s^{-1} is the stellar wind velocity. Additional lateral bending is produced by Coriolis forces, which grow with the cylindrical radius ϱ_c with respect to the star. In our model, we assume that the effect of the Coriolis force dominates the dynamics in regions where $\varrho_c > d$; these regions are further rotated by an angle $\omega_{\rm orb}(\varrho_c - d)/(2u_{\rm w})$. The resulting structure thus forms an asymmetrical spiral at large distances.

The distance to the Coriolis shock $\sim r_{\rm cor}$ is estimated analytically by equating the total pulsar wind pressure to the stellar-wind ram pressure due to the Coriolis forces [1, see their Eq. (6)]. For a realistic geometry that scales consistently with hydrodynamical simulations, we model the Coriolis shock as a spherical cap centered at the star with radius $\sim 3.3r_{\rm cor}$ [4, 5].

A conceptual diagram derived from simulations is shown in Fig. 1. The emitting region largely scales with the orbital phase for eccentric orbits, extending from approximately 2 to 7 times the semimajor axis at periastron and apastron, respectively. Thus, the processes related to the two-wind interaction proceed under different physical conditions at different orbital phases. Besides the angular effects related to orbit-induced bending, our semi-analytical modeling also accounts for relativistic effects related to the acceleration of the shocked flow, which reaches high Lorentz factors at the trailing edge of the contact discontinuity. The orbital parameters are consistent with those of LS 5039: eccentricity $e = 0.35$, orbital period $T = 3.91$ d, and semimajor axis $\alpha = 2.2 \times 10^{12}$ cm. The wind parameters that determine the shape and location of the emitting regions are the pulsar spin-down power $L_{\rm sp} = 10^{37}$ ergs^{-1} and the stellar-wind mass-loss rate $\dot{M} = 10^{-7}\ M_\odot$yr^{-1}. The inclination of the system with respect to the line of sight is fixed at 60°.

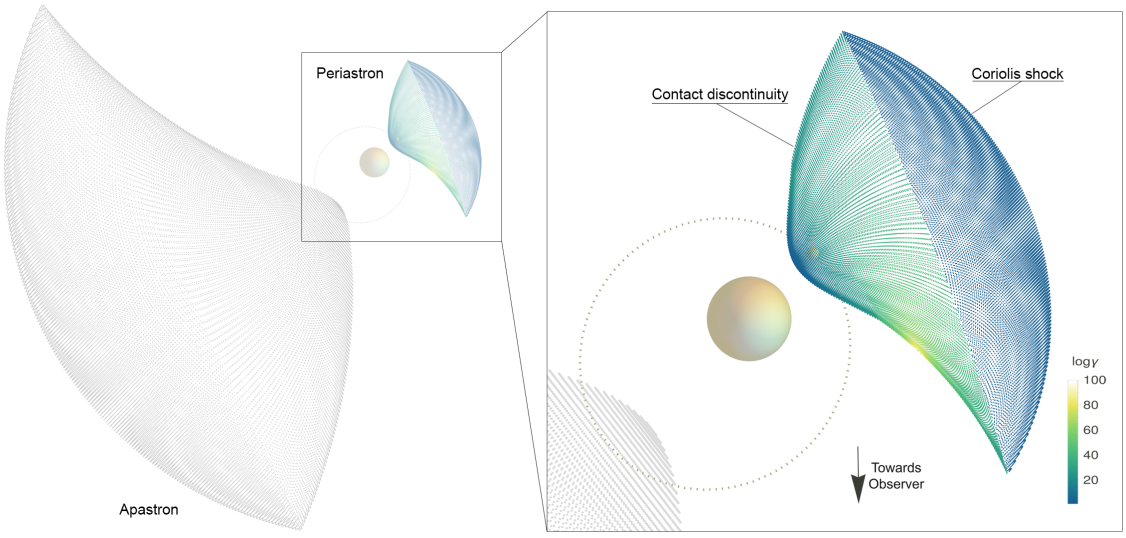

Figure 1: Simulation of the entire two-wind interaction structure at periastron and apastron (left) and zoomed-in view of the emitting region at periastron (right). The color gradient indicates the Lorentz factor of the shocked flow.

3. Application to LS 5039

The non-thermal emission is modeled by a leptonic multi-zone model considering synchrotron, inverse Compton, and γ-ray absorption and computed based on the properties of multiple emitters sampled across the contact discontinuity and the Coriolis shock. However, the reacceleration of the flow necessitates an understanding of the dominant cooling processes in each region. Close to the apex, the emitting region is radiative, but downstream of the shock, adiabatic cooling becomes important. Therefore, an additional term $-E'/t'_{\rm esc}$ is included to account for adiabatic losses. The escape timescale in the flow frame is taken as $t'_{\rm esc} = r_{\rm p}/(u_{\rm f}\gamma)$, where $r_{\rm p}$ is the distance of each emitter from the pulsar and $u_{\rm f}$ and γ are the velocity and Lorentz factor of the flow. The shocked pulsar-wind material moves parallel to the streamlines of the post-shock flow along the contact discontinuity at an approximate velocity $u_{\parallel} = c\sin\theta$, where c is the speed of light and θ is the angle between the radial direction with respect to the pulsar and the local tangential to the contact discontinuity. At the Coriolis shock, the shocked flow velocity is normal to the shock surface and taken as $c/3$.

The obtained spectral energy distributions at superior and inferior conjunction and the light curves at different energy bands are shown in Fig. 2 and Fig. 3, respectively. The adopted particle distribution is a simple power law with an index $p = 1.2$ and an exponential cutoff at $E'_{\rm cut} = 3E'_{\rm max}$. The maximum electron energy $E'_{\rm max}$ is taken as the minimum between the Hillas energy $E'_{\rm Hillas} = qB'd$ and the energy $E'_{\rm cool}$ obtained by equating the acceleration timescale $t'_{\rm acc} = E'/(\eta_{\rm acc}qcB')$ with the total radiation cooling timescale, where q is the electron charge and $\eta_{\rm acc}$ is the acceleration efficiency. The minimum energy is fixed at $E'_{\rm min} = 1$ GeV. The magnetization with respect to the pulsar-wind ram pressure is $\eta_{\rm B} = 0.3$, and the acceleration efficiency factor is $\eta_{\rm acc} = 0.5$

Our preliminary results agree reasonably well with observed data, particularly in the case

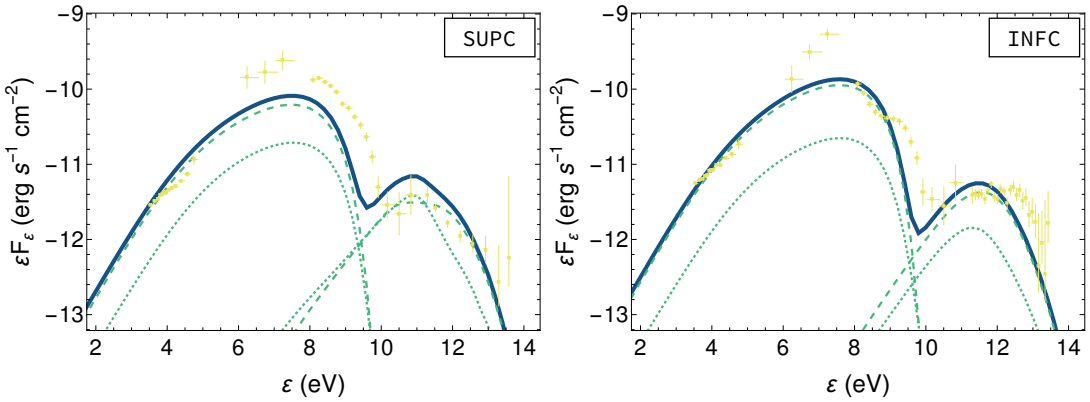

Figure 2: Modeled (blue line) and observed (yellow points) averaged spectral energy distributions at (a) superior (SUPC) and (b) inferior (INFC) conjunction. The dashed and dotted lines denote the contact discontinuity and Coriolis shock contributions, respectively.

of X-rays and very-high-energy gamma rays, and are consistent with previous works [6–9]. The X-ray emission from LS 5039 is primarily dominated by the Coriolis shock. Although the Suzaku light curve is adequately replicated by our model, the spectral energy distribution may be better fitted by a broken power law with a hard high-energy component, directly related to the complex particle acceleration processes in these sources. In the MeV band, our model captures the relative light-curve behavior, but the computed fluxes fail to reach the observed flux levels. A lower-energy component dominated by inverse Compton losses, possibly associated with the unshocked pulsar wind, is also needed to properly explain the GeV emission. Finally, TeV emission mainly originates from the Coriolis shock, where $\gamma\gamma$ absorption is less relevant. The trend in the TeV light curves matches observations and reproduces the characteristic double-peak feature reasonably.

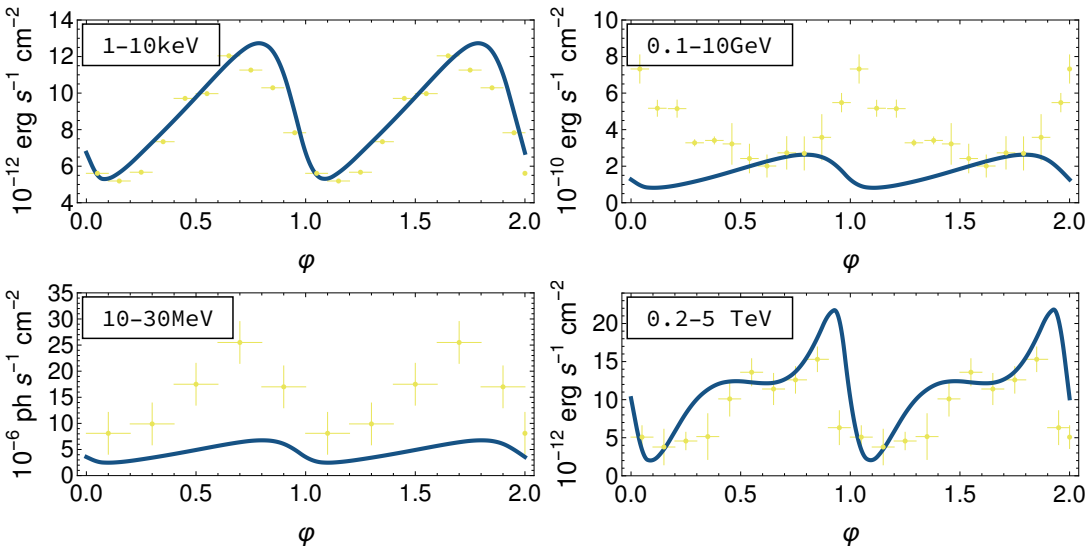

Figure 3: Modeled (blue line) and observed (yellow points) light curves for the X-ray (1 – 10 keV, Suzaku; top left), MeV (10 – 30 MeV, COMPTEL; bottom left), GeV (0.1 – 1 GeV, Fermi/LAT; top right), and TeV (0.2 – 5 TeV, H.E.S.S.; bottom right) bands.

4. Conclusions

Our semi-analytical approach considers the dynamics of the two shock regions—namely, the contact discontinuity and the Coriolis shock—resulting from the interaction between the stellar and pulsar winds. The model incorporates relativistic effects, orbital-induced bending of the two-wind structure, and realistic geometries to simulate the emitting regions and the associated high-energy emission. The application of our model to LS 5039 yields spectral energy distributions and light curves that reasonably match observational data, particularly in X-rays and very-high-energy gamma rays. However, challenges persist in accurately reproducing the observed behavior across all energy bands. The discrepancy between the predicted MeV/GeV emission and the actual data indicates limitations in our understanding of the underlying physical processes and the need for refinements in the modeling approach.

Acknowledgments

This work has received financial support from the State Agency for Research of the Spanish Ministry of Science and Innovation under grant PID2022-136828NB-C41 and through the "Unit of Excellence María de Maeztu 2020–2023" award to the Institute of Cosmos Sciences (CEX2019-000918-M). V.B-R. is Correspondent Researcher of CONICET, Argentina, at the IAR.

References

[1] V. Bosch-Ramon and M.V. Barkov, *Large-scale flow dynamics and radiation in pulsar γ-ray binaries*, *A&A* **535** (2011) A20.

[2] V. Zabalza, V. Bosch-Ramon, F. Aharonian and D. Khangulyan, *Unraveling the high-energy emission components of gamma-ray binaries*, *A&A* **551** (2013) A17.

[3] J. Cantó, A.C. Raga and F.P. Wilkin, *Exact, algebraic solutions of the thin-shell two-wind interaction problem*, *ApJ* **469** (1996) 729.

[4] V. Bosch-Ramon, *Properties of a hypothetical cold pulsar wind in LS 5039*, *A&A* **645** (2021) A86.

[5] R. Kissmann, D. Huber and P. Gschwandtner, *High-resolution simulations of LS 5039*, *A&A* **677** (2023) A5.

[6] G. Dubus, A. Lamberts and S. Fromang, *Modelling the high-energy emission from gamma-ray binaries using numerical relativistic hydrodynamics*, *A&A* **581** (2015) A27.

[7] E. Molina and V. Bosch-Ramon, *A dynamical and radiation semi-analytical model of pulsar–star colliding winds along the orbit: Application to LS 5039*, *A&A* **641** (2020) A84.

[8] D. Huber, R. Kissmann and O. Reimer, *Relativistic fluid modelling of gamma-ray binaries - II. application to LS 5039*, *A&A* **649** (2021) A71.

[9] H. Yoneda, D. Khangulyan, T. Enoto, K. Makishima, K. Mine, T. Mizuno et al., *Broadband high-energy emission of the gamma-ray binary system LS 5039: Spectral and temporal features using NuSTAR and Fermi observations*, *ApJ* **917** (2021) 90.